J. Fluid Mech. (1988), *vol.* 190, *pp.* 393–407
Printed in Great Britain

Numerical modelling of nonlinear effects in laminar flow through a porous medium

By O. COULAUD†‡, P. MOREL† AND J. P. CALTAGIRONE‡

† UER de Mathématiques, Mathématiques Appliquées, LA au CNRS 226, 351, Cours de la Libération, 33405 Talence Cedex, France

‡ Laboratoire d'Energétique et Phénomènes de Transfert, UA CNRS 873, Esplanade des Arts et Métiers, 33405 Talence Cedex, France

(Received 23 February 1987 and in revised form 13 August 1987)

This paper deals with the introduction of a nonlinear term into Darcy's equation to describe inertial effects in a porous medium. The method chosen is the numerical resolution of flow equations at a pore scale. The medium is modelled by cylinders of either equal or unequal diameters arranged in a regular pattern with a square or triangular base. For a given flow through this medium the pressure drop is evaluated numerically.

The Navier–Stokes equations are discretized by the mixed finite-element method. The numerical solution is based on operator-splitting methods whose purpose is to separate the difficulties due to the nonlinear operator in the equation of motion and the necessity of taking into account the continuity equation. The associated Stokes problems are solved by a mixed formulation proposed by Glowinski & Pironneau.

For Reynolds numbers lower than 1, the relationship between the global pressure gradient and the filtration velocity is linear as predicted by Darcy's law. For higher values of the Reynolds number the pressure drop is influenced by inertial effects which can be interpreted by the addition of a quadratic term in Darcy's law.

On the one hand this study confirms the presence of a nonlinear term in the motion equation as experimentally predicted by several authors, and on the other hand analyses the fluid behaviour in simple media. In addition to the detailed numerical solutions, an estimation of the hydrodynamical constants in the Forchheimer equation is given in terms of porosity and the geometrical characteristics of the models studied.

1. Introduction

For a single-phase flow, a pressure gradient imposed upon a porous medium induces a given filtration velocity. Darcy (1856) observed that when this velocity is relatively small, it is proportional to the pressure gradient. When the filtration velocity is larger, leading to Reynolds numbers greater than one, the measured pressure drop exceeds the value predicted by Darcy's law. The existence of this phenomenon, as shown by several authors (Dupuit 1863; Forchheimer 1901; Irmay 1958; Chauveteau 1965; Beavers & Sparrow 1969; Beavers, Sparrow & Rodenz 1973; de Vries 1979), requires the introduction of a corrective quadratic term in Darcy's equation.

The importance of this phenomenon in applications of both forced flow and natural convection currents is the motivation for this study. For the case of natural

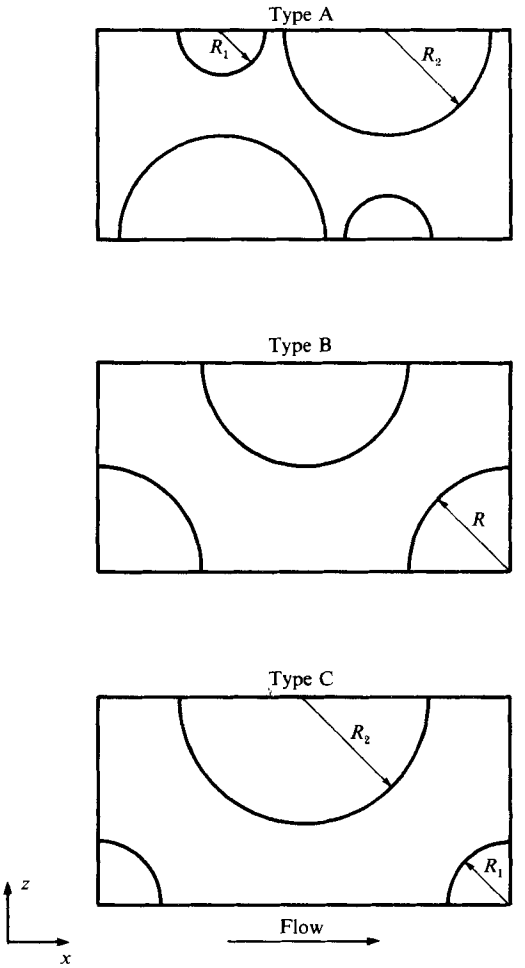

FIGURE 1. Definition of the different base cells.

convection the quadratic terms influence both the flow stability and the convective structure (Catton 1984; Nield & Joseph 1985).

The introduction of an inertial term of the type $((\boldsymbol{V}\cdot\boldsymbol{\nabla})\,\boldsymbol{V})$ in Darcy's equation is not entirely satisfactory; indeed, if one considers a unidirectional flow, this term is reduced to zero independently of the Reynolds number. This type of formulation, based only on the filtration velocity is unsatisfactory because it does not take into account inertial effects at the pore scale; see, for example, Whitaker (1969).

The usual formulation used to model these phenomena is Forchheimer's law, which includes a nonlinear term of the form $C\rho K^{-\frac{1}{2}}|\boldsymbol{V}|\cdot\boldsymbol{V}$ in Darcy's equation. The constant C associated with the nonlinear term depends only on the geometry of the porous medium. Knowledge of C is necessary in order to determine the velocity field when inertial effects are important.

In order to pursue this approach, pressure and velocity fields are calculated for a porous medium modelled in terms of cylinders arranged in a regular pattern as illustrated in figures 1 and 2. The determination of velocities and pressure at each point of the domain, as well as the global pressure drop, will not only help the

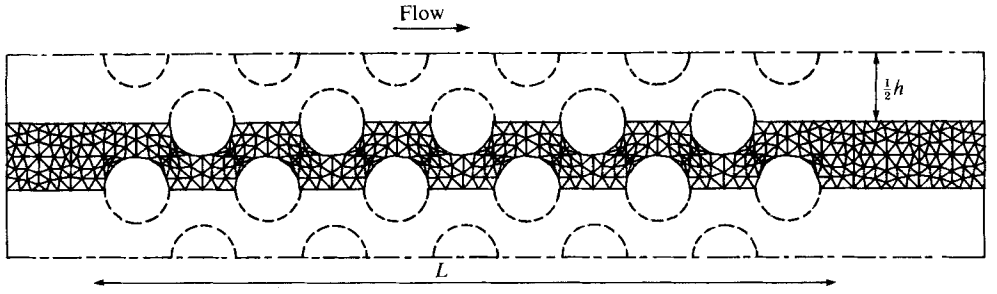

FIGURE 2. Network configuration.

understanding of the physical mechanisms involved but will also enable the calculation of the global characteristics as a function of the Reynolds number.

With high performance of computers and algorithms, numerical flow simulations can accommodate complex geometric structures. Thus it is possible to analyse the motion at the pore scale to obtain some information on the relative magnitude of recirculation in the pore and on the repartitioning of the pressure at the substrate surface. The few simplistic cases that have been solved can aid the understanding of the real media.

2. Formulation of the problem

Consider a porous medium of length L in the x-direction and of infinite length in the y- and z-directions, modelled by a periodic network of cylinders with axes parallel to the y-direction. For this situation the local velocity can be represented as

$$\boldsymbol{v} = u\boldsymbol{e}_x + w\boldsymbol{e}_z,$$

where $\boldsymbol{e}_x$ and $\boldsymbol{e}_z$ are respectively the unit base vectors in the x- and z-directions. The porous medium is composed of a series of cells translated from a basic cell. The calculation domain Ω includes the model porous medium bounded upstream and downstream by fluid volumes as illustrated in figure 2.

The fluid circulating through this system is assumed to be incompressible with a density ρ and a constant viscosity μ. The velocity $\boldsymbol{v}$ and the pressure p are governed by Navier–Stokes and continuity equations which we express as

$$\rho\left(\frac{\partial \boldsymbol{v}}{\partial t} + (\boldsymbol{v}\cdot\nabla)\,\boldsymbol{v}\right) = -\nabla p + \mu\nabla^2\boldsymbol{v} \qquad \text{in } \Omega, \tag{2.1}$$

$$\nabla\cdot\boldsymbol{v} = 0 \qquad \text{in } \Omega. \tag{2.2}$$

The boundary conditions of the problem are

$$\left.\begin{aligned} u = w \quad &= 0 \quad \text{on } \Gamma_1, \text{ at the surface of the cylinder,} \\ \frac{\partial u}{\partial z} = w \quad &= 0 \quad \text{on } \Gamma_2, \text{ at the lines of symmetry,} \\ u = V_0, \quad w = 0 \quad &\text{on } \Gamma_3, \text{ at the entry and at the exit.} \end{aligned}\right\} \tag{2.3}$$

By solving this set of equations we obtain not only the pressure and velocity fields but also, by numerical integration, the global values of the pressure drop. In this way

we are able to obtain an equation which incorporates a quadratic term into Darcy's equation according to

$$\nabla P + \mu K^{-1} V + C\rho K^{-\frac{1}{2}} |V| \cdot V = 0, \tag{2.4}$$

where K represents the component $\boldsymbol{e}_x \cdot \boldsymbol{K} \cdot \boldsymbol{e}_x$ where $\boldsymbol{K}$ is the Darcy's law permeability tensor.

For computational purposes the equations and the boundary conditions need to be represented in non-dimensional form. The space coordinates are normalized by the average diameter d of the cylinders, the velocity by the average entry velocity V_0, the pressure by ρV_0^2 and the time by d/V_0. For the convenience of the reader we have used the same symbols for the dimensionless pressure and velocity as we have used for the dimensional quantities given earlier in (2.1), (2.2) and (2.4). The dimensionless system is given by

$$\nabla \cdot \boldsymbol{v} = 0, \tag{2.5}$$

$$\frac{\partial \boldsymbol{v}}{\partial t} + (\boldsymbol{v} \cdot \nabla)\, \boldsymbol{v} = -\nabla p + \frac{1}{\mathrm{Re}} \nabla^2 \boldsymbol{v}, \tag{2.6}$$

where $Re = V_0 d\rho/\mu$ is a Reynolds pore number.

$$\left.\begin{aligned} \boldsymbol{v} &= 0 && \text{at the surface of the cylinders,} \\ \boldsymbol{v} &= \boldsymbol{e}_x && \text{at the entry and at the exit,} \\ \frac{\partial}{\partial z}(\boldsymbol{v} \cdot \boldsymbol{e}_x) &= \boldsymbol{v} \cdot \boldsymbol{e}_z = 0 && \text{along the lines of symmetry.} \end{aligned}\right\} \tag{2.7}$$

The dimensionless form of the local volume-average equations is given by

$$\nabla \cdot V = 0, \tag{2.8}$$

$$\nabla P + (Re\, K/d^2)^{-1} V + C(K/d^2)^{-\frac{1}{2}} |V| \cdot V = 0. \tag{2.9}$$

The term K/d^2 can be considered as a combination of a Darcy number, K/h^2 for example, and a form ratio of h/d.

The system of equations (2.5)–(2.7) yields the pressure field for the model medium and defines, by exact numerical integration over plane sections (x = constant), the average pressure. The entry velocity V_0 being given, starting from the overall pressure drop through the model, an identification procedure allows the estimation of the Forchheimer coefficient for the three geometric situations that have been chosen for study.

3. Numerical algorithm

The algorithm that is discussed hereafter is an adaptation to the type of boundary conditions considered in this problem (symmetry conditions) of the method proposed by Glowinski & Pironneau (1978, 1979); Glowinski (1984); Bristeau *et al.* (1979).

3.1. *Time discretization by operator-splitting methods*

Two difficulties are encountered in solving the system (2.1)–(2.3): (i) the nonlinear term $(\boldsymbol{v} \cdot \nabla)\, \boldsymbol{v}$ in the equation of motion; (ii) the incompressibility condition $\nabla \cdot \boldsymbol{v} = 0$. These two problems are uncoupled by use of operator-splitting methods for the time

discretization. Consider the affine functional space $\mathbb{V}_g$ of sufficiently regular functions $\boldsymbol{v}$, such that $\boldsymbol{v} = \boldsymbol{g}$ on $\Gamma' = \Gamma_1 \cup \Gamma_3$, $\boldsymbol{v}\cdot\boldsymbol{n} = 0$ on Γ_2 and the compatibility condition

$$\int_{\Gamma'} \boldsymbol{g}\cdot\boldsymbol{n}\,\mathrm{d}\sigma = 0.$$

Two operators A_1 and A_2 are defined by

$$A_1 \boldsymbol{v} = -\frac{2}{3Re}\nabla^2 \boldsymbol{v}, \tag{3.1}$$

$$A_2(\boldsymbol{v}) = (\boldsymbol{v}\cdot\nabla)\,\boldsymbol{v} - \frac{1}{3Re}\nabla^2 \boldsymbol{v}, \tag{3.2}$$

where A_1 is a linear operator and A_2 is a nonlinear one. Let Δt (> 0), be the time discretization step. We define the following scheme by:

$$\text{let } v^0 \text{ be given and for all } n > 0,\ v^{n+1} \text{ is calculated by} \tag{3.3}$$

step 1

$$\left.\begin{aligned} \frac{4}{\Delta t}(\boldsymbol{v}^{n+\frac{1}{4}} - \boldsymbol{v}^n) + A_1 \boldsymbol{v}^{n+\frac{1}{4}} + \nabla p^{n+\frac{1}{4}} &= A_2(\boldsymbol{v}^n), \\ \nabla\cdot\boldsymbol{v}^{n+\frac{1}{4}} &= 0, \\ \boldsymbol{v}^{n+\frac{1}{4}} \in \mathbb{V}_g,\quad \frac{\partial}{\partial n}(\boldsymbol{v}^{n+\frac{1}{4}}\cdot\boldsymbol{\tau}) &= 0 \quad \text{on } \Gamma_2; \end{aligned}\right\} \tag{3.4}$$

step 2

$$\left.\begin{aligned} \frac{2}{\Delta t}(\boldsymbol{v}^{n+\frac{3}{4}} - \boldsymbol{v}^{n+\frac{1}{4}}) + A_2 \boldsymbol{v}^{n+\frac{3}{4}} &= A_1 \boldsymbol{v}^{n+\frac{1}{4}} - \nabla p^{n+\frac{1}{4}} \\ \boldsymbol{v}^{n+\frac{3}{4}} \in \mathbb{V}_g,\quad \frac{\partial}{\partial n}(\boldsymbol{v}^{n+\frac{3}{4}}\cdot\boldsymbol{\tau}) &= 0 \quad \text{on } \Gamma_2; \end{aligned}\right\} \tag{3.5}$$

step 3

$$\left.\begin{aligned} \frac{4}{\Delta t}(\boldsymbol{v}^{n+1} - \boldsymbol{v}^{n+\frac{3}{4}}) + A_1 \boldsymbol{v}^{n+1} + \nabla p^{n+1} &= A_2(\boldsymbol{v}^{n+\frac{3}{4}}), \\ \nabla\cdot\boldsymbol{v}^{n+1} &= 0, \\ \boldsymbol{v}^{n+1} \in \mathbb{V}_g,\quad \frac{\partial}{\partial n}(\boldsymbol{v}^{n+1}\cdot\boldsymbol{\tau}) &= 0 \quad \text{on } \Gamma_2; \end{aligned}\right\} \tag{3.6}$$

where $\boldsymbol{v}^j = \boldsymbol{v}(x, j\Delta t)$; $p^j = p(x, j\Delta t)$; $\boldsymbol{\tau}$ is the unit tangent vector at Γ_2.

Steps 1 and 3 yield respectively $\boldsymbol{v}^{n+\frac{1}{4}}$, $p^{n+\frac{1}{4}}$ and $\boldsymbol{v}^{n+1}$, p^{n+1} by solving for each time an unsteady Stokes problem with mixed-type boundary conditions. Step 2 gives $\boldsymbol{v}^{n+\frac{3}{4}}$ by solving a nonlinear problem. The scheme (3.3)–(3.6) is second-order accurate (Bristeau *et al.* 1979).

3.2. *Solving the nonlinear problem*

The method of least squares (Bristeau *et al.* 1979; Glowinski 1984) is used to solve (3.5); thus instead of seeking $\boldsymbol{v}$ as the solution of this equation, it is sought as the solution to a minimization problem. This solution is approached by a conjugated gradient algorithm.

For given $v \in \mathbb{V}_g$ the function $y(v)$ is defined as the unique solution of

$$\left.\begin{aligned} &\left(\frac{2}{\Delta t} I - \frac{1}{3Re}\nabla^2\right) y = \left(\frac{2}{\Delta t} I - \frac{1}{3Re}\nabla^2\right) v + (v\cdot\nabla)\, v - f, \\ &y \in \mathbb{V}_0, \quad \frac{\partial}{\partial n}(y\cdot\tau) = 0 \quad \text{on } \Gamma_2. \end{aligned}\right\} \tag{3.7}$$

We note that v is the solution of (3.5) if and only if y is identical to zero. The functional $J(v)$ is then defined by the following expression:

$$J(y) = \frac{1}{2}\int_\Omega \left\{\frac{2}{\Delta t}|y|^2 + \frac{1}{3Re}|\nabla y|^2\right\} dx, \tag{3.8}$$

and the minimization problem as: Find $v \in \mathbb{V}_g$ such that

$$J(v) > J(w)\ \forall\, w \in \mathbb{V}_g. \tag{3.9}$$

The Polak–Ribière (Polak 1971) version of the conjugate gradient method is used to solve (3.9). The only important step in this algorithm is the calculation of the differential of J.

3.3. *Solving the Stokes problems*

For each step of the scheme given by (3.3)–(3.6) two Stokes problems corresponding to steps 1 and 3 have to be solved. These are of the following type:

$$\left.\begin{aligned} \left(\frac{4}{\Delta t} I - \frac{2}{3Re}\nabla^2\right) v + \nabla p &= f \quad \text{in } \Omega, \\ \nabla\cdot v &= 0, \quad \text{in } \Omega, \\ v \in \mathbb{V}_g, \quad \frac{\partial}{\partial n}(v\cdot\tau) &= 0 \quad \text{on } \Gamma_2. \end{aligned}\right\} \tag{3.10}$$

This linear problem is solved by applying the decomposition method of the Stokes operator as proposed by Glowinski & Pironneau (1978, 1979) as a cascade of Poisson's equations. We use the following computational routine:

Find p_0 such that

$$\left.\begin{aligned} -\nabla^2 p_0 &= -\nabla\cdot f \quad \text{in } \Omega, \\ p_0 &= 0 \quad \text{on } \Gamma. \end{aligned}\right\} \tag{3.11}$$

Find u_0 such that

$$\left.\begin{aligned} \left(\frac{4}{\Delta t} I - \frac{2}{3Re}\nabla^2\right) u_0 &= f - \nabla p_0 \quad \text{in } \Omega, \\ u_0 \in \mathbb{V}_g, \quad \frac{\partial}{\partial n}(u_0\cdot\tau) &= 0 \quad \text{on } \Gamma_2. \end{aligned}\right\} \tag{3.12}$$

Find ϕ_0 such that

$$\left.\begin{aligned} -\nabla^2\phi_0 &= -\nabla\cdot u_0 \quad \text{in } \Omega, \\ \phi_0 &= 0 \quad \text{on } \Gamma. \end{aligned}\right\} \tag{3.13}$$

Solve

$$A\lambda = \partial\phi_0/\partial n. \tag{3.14}$$

Find $\bar{p}$ such that

$$\left.\begin{aligned} -\nabla^2\bar{p} &= 0 \quad \text{in } \Omega, \\ p &= \lambda \quad \text{on } \Gamma. \end{aligned}\right\} \tag{3.15}$$

Find $\boldsymbol{u}$ such that

$$\left.\begin{aligned} &\left(\frac{4}{\Delta t}I-\frac{2}{3Re}\nabla^2\right)\boldsymbol{u}=-\nabla\bar{p} \quad \text{in } \Omega,\\ &\boldsymbol{u}\in\mathbb{V}_0, \quad \frac{\partial}{\partial n}(\boldsymbol{u}\cdot\boldsymbol{\tau})=0 \qquad \text{on } \Gamma_2. \end{aligned}\right\} \tag{3.16}$$

Then the solution of (3.10) is given by

$$p=\bar{p}+p_0, \quad \boldsymbol{v}=\boldsymbol{u}+\boldsymbol{u}_0.$$

In (3.14), A is a boundary operator which gives the pressure on the boundary that is required in order to have $\nabla\cdot\boldsymbol{v}=0$. The discrete version of A is presented in the pendix. The notation is introduced in §3.4 below. For more details see Glowinski Pironneau (1978, 1979); Glowinski (1984); Thomasset (1980).

3.4. *Discretization in space*

The domain is discretized by a regular triangularization T_h. The approximation is carried out by the mixed finite-elements method of the Lagrange type. Our objective is the solution of the Navier–Stokes equations to obtain the pressure and velocity fields from which we can calculate the area-averaged values. An approximation space P_1 is chosen for the pressure while an approximation space P_2 is used for the components of the velocity field. The average pressure on the segment, $(x,y)\in R^2$, with $x=$ constant and $a(x)\leqslant y\leqslant b(x)$ is defined by

$$P_m(x)=[b(x)-a(x)]^{-1}\int_{a(x)}^{b(x)} p_h(x,y)\,dy, \tag{3.17}$$

where p_h is the finite-element approximation of the pressure.

By interpolation, the pressure takes the form of a piece-wise polynomial of the first degree. In (3.17) we use a quadrature formula (3.18) which is exact for polynomial of the first degree:

$$\int_a^b f(x,y)\,dy=\tfrac{1}{2}(b-a)\,[f(x,a)+f(x,b)]. \tag{3.18}$$

Solving the Navier–Stokes equations by this method is carried out using the Modulef finite-elements code (Conca & Steer 1983; Modulef 1984). We have carried out calculations on different grids in order to indicate under what circumstances the results are grid-independent. We show in figure 2 the triangularization used in these calculations, and for that case we have 2587 unknowns for one component of the velocity and 712 for the pressure. We assumed that the steady solution is obtained when the relative maximum of the increment of the pressure between step 1 and step 3 is less than $10^{-4}\,\Delta t$. To obtain this convergence we need (with $\Delta t=10^{-2}$) 18 iterations for $Re=1$ and 365 for $Re=20$. Each time step requires about 3.5 s on an IBM 3081.

4. Presentation and interpretation of the results

4.1. *Geometrical patterns*

Three different geometries A, B, C, illustrated in figure 1, are used as model porous media. The first two are regular networks of cylinders in either a triangular or a square array. The third has a different shape, i.e. diameter; so in the result we can hope to see some influence of the lattice design and the shape.

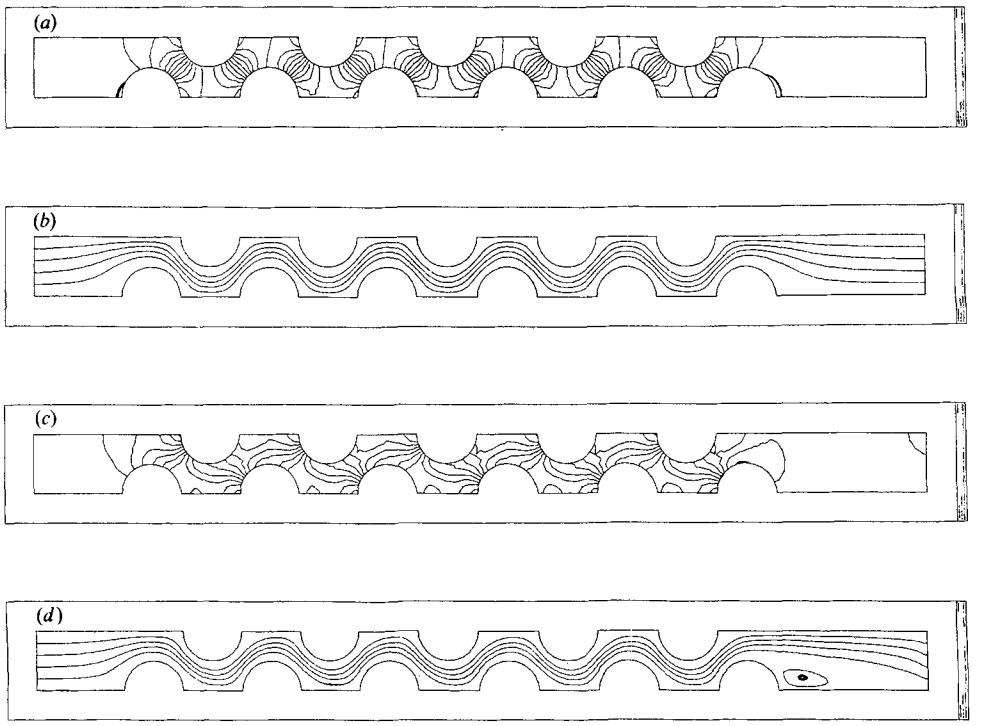

FIGURE 3. (*a*) Isobar lines for $Re = 1$; (*b*) streamlines for $Re = 1$; (*c*) isobar lines for $Re = 20$; (*d*) streamlines for $Re = 20$.

We are not only interested in the behaviour of the pressure and the streamlines in the porous medium, but also the influence of the position of the fluid–solid interface on the pressure drop. Thus the computational domain must contain a long line of cylinders and 'calming' zones before and after the pattern illustrated in figure 2. The latter allows the velocities at the entry and exit of the domain to be set equal to each other.

4.2. *Pressure fields and streamlines*

The local pressure fields and streamlines are obtained in detail for a B-type pattern, with the dimensionless cylinder diameter equal to 1, i.e. a porosity $\epsilon = 0.61$. The solution to the Navier–Stokes equations for Reynolds numbers higher than 10 are obtained by an incremental process. Two streamline and isobar-line networks are presented in figure 3(*a–d*) for Reynolds numbers of 1 and 20.

We first examined the location of the point where pressure is a minimum. It situated at the back of the cylinder for $Re = 1$, but when Re increases to 20 it is shifted to a point situated at an angle of 100° (direct orientation). This change is due to the recirculation of the fluid downstream of the pattern just behind the last cylinder, as illustrated in figure 3(*d*). The point of maximum pressure, however, remains located in the same place, situated on the first cylinder. The arrangement of the isobars in the interior of the flow pattern is quite different for the two Reynolds numbers. In the case $Re = 1$, the isobars are distributed in a symmetrical fashion between two adjacent cylinders. In addition, the network is perfectly symmetrical with respect to the straight line $x = \frac{1}{2}L$, where L is the length of the model porous medium and is 16 for A, 11 for B and 17 for C. In the case $Re = 20$ the network, as

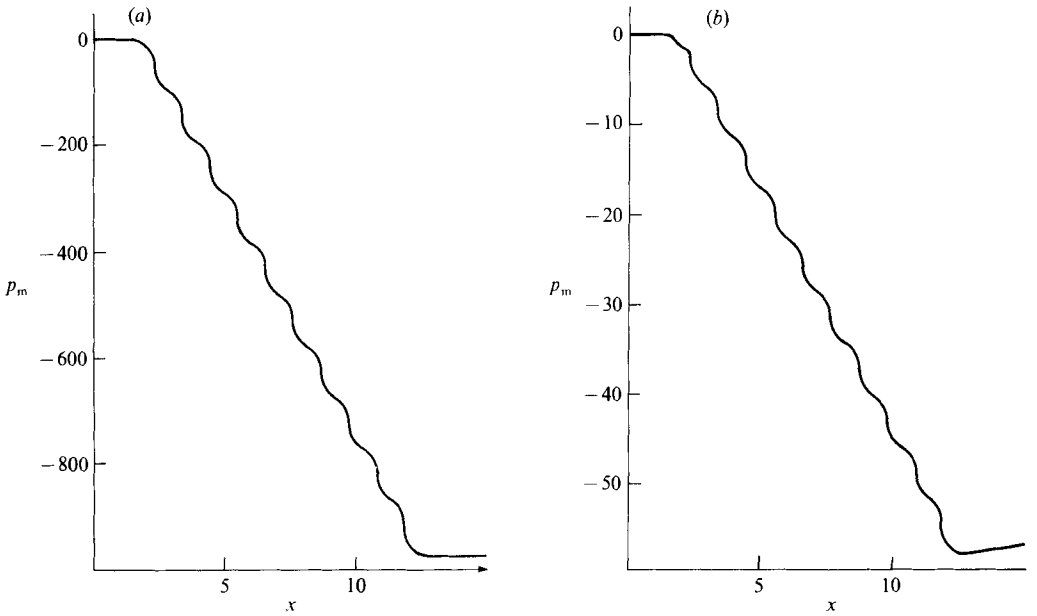

FIGURE 4. Evolution of average pressure for (*a*) $Re = 1$; (*b*) 20.

a whole, is not symmetric. Some isobar lines remain situated close to the straight line joining the centres of two adjacent cylinders, but with a distribution that is no longer symmetric. Isobar lines situated on the left will shift towards the front of the other cylinder as will those on the right. It can be noted that when the Reynolds number increases, the first isobar located behind the maximum point moves to the front of the cylinder to a limit position corresponding to an angle of $\frac{3}{4}\pi$.

The evolution of the average pressure shown in figure 4 is calculated by integrating the pressure at x = constant. In the two cases considered here, it can be noted that the average pressure remains constant in the region $0 \leqslant x \leqslant 1.5$. At the exit, however, only for the case where the Reynolds number equals one is the global pressure constant. When $Re = 20$, an increase in the average pressure can be seen, owing to the recovery of kinetic energy associated with the appearance of a vortex behind the last cylinder. The latter has a value of -980 for a Reynolds number of 1 and -58 for $Re = 20$. Also to be noted is the constant value of the average slope of the pressure gradient in the network. Thus the result is the classical one for the variation of average pressure of a uniform flow in a porous medium : that the pressure is uniform in the upstream zone and in the downstream zone, the profile being linear inside the medium.

4.3. *Nonlinear effects*

The evolution of the average pressure variation $-\Delta p$, as a function of the Reynolds number Re, is given in the case of a type-A pattern for the porosity of 0.43. This is different from the example presented in a previous publication (Coulaud, Morel & Caltagirone 1986). In order to facilitate the determination of the numerical constants, the evolution of $(-\Delta p\, Re\, d/L)$ is plotted as a function of Re. For a more convenient presentation of the results, the curve is normalized by the value, α, of $(-\Delta p\, Re\, d/L)$ at $Re = 0$ which is virtually constant. In this case $\alpha = 188.8$. By normalizing with respect to α, figure 5 is obtained. This plot can be decomposed into

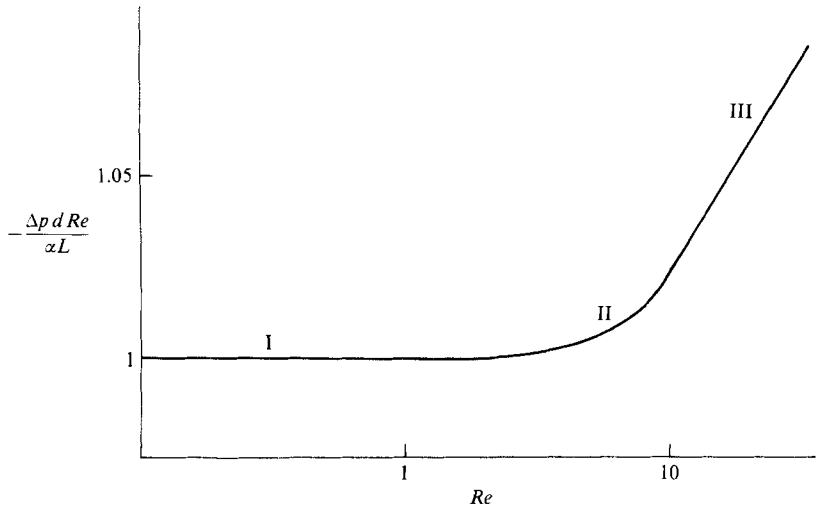

FIGURE 5. Influence of the Reynolds number, type A, $\epsilon = 0.43$.

three zones: the first, for $Re \leqslant 1$; the second, for $1 < Re \leqslant Re_c$ with Re_c lying between 13 and 14; and the third, for $Re_c < Re \leqslant 25$.

In the first zone ($Re \leqslant 1$) there exists a linear relationship between the average pressure gradient and the filtration velocity. This relationship is given by

$$-\frac{\partial p}{\partial x} = \mu\left(\frac{\alpha}{d^2}\right) v_0, \tag{4.1}$$

in which p is the area-averaged pressure. By comparing this to Darcy's law, the permeability of the equivalent porous medium being studied is obtained and the permeability is given by $K = d^2/\alpha$.

The second zone is a transition zone. The effects arising from the inertial terms of the Navier–Stokes equations are no longer negligible.

In the third zone ($Re \geqslant 13$–14) an affine relationship is observed:

$$\frac{-\Delta p\, d\, Re}{\alpha L} = a\, Re + b, \tag{4.2}$$

where $$a = 0.005 \quad \text{and} \quad b = 0.97.$$

Coming back to real magnitudes, the following relationship is obtained:

$$-\frac{\partial p}{\partial x} \approx -\frac{\Delta p}{L} = \frac{a\alpha}{d}\rho v_0^2 + \frac{b\alpha}{d^2}\mu v_0. \tag{4.3}$$

This shows that the average pressure gradient is a quadratic function of the filtration velocity, analogous to Forchheimer's law (2.4), where $C = a(\alpha/b)^{\frac{1}{2}}$.

4.4. *Influence of porosity*

The influence of porosity on $-\Delta p\, Re$ as a function of the Reynolds number is studied for type A and B patterns. The curves are normalized with respect to the coefficient α in order to make the comparison possible. Interpretations of the normalized curves are made for three porosities: $\epsilon = 0.43$, 0.61 and 0.80. The results are shown in figure 6(a, b).

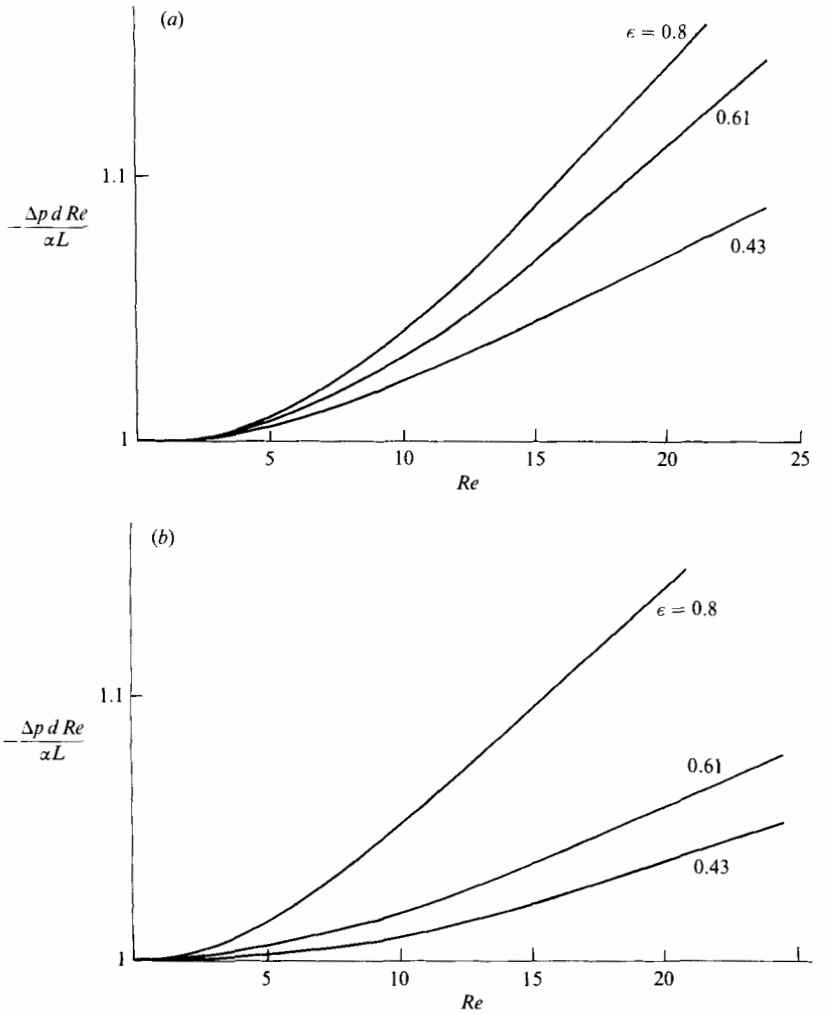

FIGURE 6. (*a*) Influence of porosity: (*a*) type A; (*b*) type B.

It can be seen that in both of these cases the function $(-\Delta pd\, Re/\alpha L)$ decreases with decreasing porosity. Tables 1–5 show the variation of some coefficients and parameters with porosity. Table 1 indicates that the coefficient a, that is the slopes for $Re_c < Re < 25$, follows the same variations as the porosity. With the aid of table 3 we see that the constant C in Forchheimer's law seems to be of the form

$$C = \frac{\text{constant}}{\epsilon} \text{ for a porosity value less than } 0.61.$$

Thus it would appear that there exists a constant C_0 which is independent of ϵ, but depends on the lattice design. It follows that, in dimensional form, the law (4.3) can be written as

$$-\frac{\partial p}{\partial x} = \frac{\mu}{k_a} V_0 + \frac{\rho}{\epsilon k_a^{\frac{1}{2}}} C_0 V_0^2; \quad k_a = \frac{d}{b\alpha}$$

when the Reynolds number is between R_c and 25.

ϵ	A	B	C
0.43	0.005	0.0087	0.004
0.61	0.008	0.014	
0.80	0.010	0.029	

TABLE 1. Coefficient a of the straight line $a\,Re+b$

ϵ	A	B	C
0.43	0.97	0.95	0.98
0.61	0.94	0.91	
0.80	0.94	0.88	

TABLE 2. Coefficient b of the straight line $a\,Re+b$

ϵ	A	B	C
0.43	0.042	0.086	0.031
0.61	0.041	0.085	
0.80	0.027	0.098	

TABLE 3. Coefficient $C_1 = C\epsilon$

ϵ	A	B	C
0.43	377.52	505.58	326.11
0.61	67.36	89.09	
0.80	10.61	15.85	

TABLE 4. Parameter α-values

ϵ	A	B	C
0.43	0.84	1.2	1.14
0.61	0.70	1.0	
0.80	0.43	0.70	

TABLE 5. Average diameter

4.5. *Influence of geometry*

At this point we examine the behaviour of the curves $(-\Delta p\,Re\,d/\alpha L)$ as a function of the Reynolds number, and also of the coefficients in (4.3) for the Reynolds numbers between R_c and 25, according to the three geometries A, B and C.

Figure 7 shows the influence of the pattern structure on the behaviour of $(-\Delta p\,Re\,d/\alpha L)$ as a function of Re. The curves resulting from the structures A and C, that is for different radii, are very nearly identical, the maximum difference between the two being 0.012 for $Re = 25$. Once more, the difference between the configurations of A, C and that of B attain a value of 0.08 for $Re = 25$. For $1 \leqslant Re \leqslant 25$ the difference is minimal.

We need to investigate further the coefficient C_0, which was first presented in §4.4

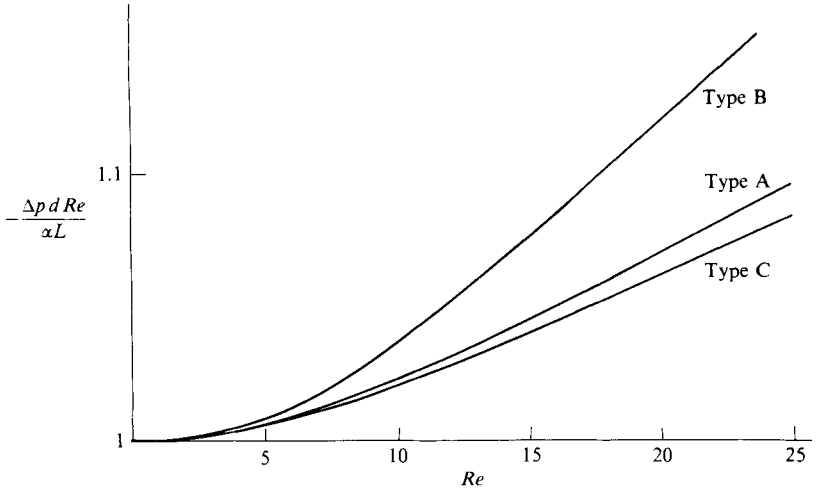

FIGURE 7. Influence of geometry: $\epsilon = 0.43$.

and also appears in Forchheimer's law. If the product $C_0 d$ is considered, where d is the average diameter of the cylinders in the basic cell, the following result is obtained:

$$\text{A} = 0.0356; \quad \text{B} = 0.103; \quad \text{C} = 0.0358.$$

In cases A and C, that is when the two curves illustrated in figure 7 are close, a constant C_1 would seem to exist where $C_0 = C_1/d$. Thus the coefficient C appearing in Forchheimer's law could be written as $C = C_1/(\epsilon d)$.

The constant C_1 cannot be said to be universal: for such a claim other types of configurations would have to be examined.

5. Conclusions

This study of a uniform flow does not furnish definite conclusions about the complementary terms to be integrated in the equation describing the fluid motion through a real porous medium and incorporating the associated inertial elements.

Nonetheless, this purely descriptive microscopic approach constitutes an interesting complement for actual experiments or for other theories such as homogenization. This work corroborates certain experiments by confirming that Darcy's and Forchheimer's laws are only valid in well-established ranges of Reynolds numbers (Bear 1972).

The numerical solution of the Navier–Stokes equations in the three model patterns allowed some direct results:

(i) the validation of the presence of quadratic terms in an equation expressing filtration velocity for Reynolds numbers that exceed a critical value Re_c close to 13 and less than 25;

(ii) the specification of the form and value of the parameters and constants associated with this term;

(iii) the determination of the different rates of the nonlinear Darcy transition flow.

It appears that the resulting nonlinear form of Darcy's law is very similar to Forchheimer's law when the porosity is small and the pattern rather complex.

This study also shows that it is not possible to define a valid universal constant independent of the geometry of the medium.

Appendix

A.1. *Construction of the operator* A

The following spaces are introduced:

$$V_h = \{q_h \,|\, q_h \in C^0(\Omega), \quad q_{h|K} \in P_1, \quad \forall K \in T_h\},$$
$$V_{0,h} = \{q_h \,|\, q_h \in V_h, \quad q_{h|\Gamma} = 0, \quad \Gamma = \Gamma_1 \cup \Gamma_2 \cup \Gamma_3\},$$
$$U_{0,h} = \{\boldsymbol{u}_h \,|\, \boldsymbol{u}_h \in C^0(\Omega) \times C^0(\Omega), \quad \boldsymbol{u}_{h|K} \in P_2 \times P_2,$$
$$\boldsymbol{u}_h = 0 \quad \text{on } \Gamma_1 \cup \Gamma_3, \quad \boldsymbol{u}_h \cdot \boldsymbol{n} = 0 \quad \text{on } \Gamma_2\}.$$

Let $(q_i)_{i=1,N}$ be a basis of V_h: q_i is the basis function relative to vertex i.

The symmetric positive definite operator A is constructed column by column.

For each vertex $i \in \Gamma$ the following problems are solved. Find $p_h^i \in q_i + V_{0,h}$ such that

$$\int_\Omega \nabla p_h^i \cdot \nabla \phi \, \mathrm{d}x = 0, \quad \phi \in V_{0,h}; \tag{A 1}$$

find $\boldsymbol{u}_h^i \in U_{0,h}$ such that

$$\alpha \int_\Omega \boldsymbol{u}_h^i \cdot \boldsymbol{V}_h \mathrm{d}x + \beta \int_\Omega \nabla \boldsymbol{u}_h^i \cdot \nabla \boldsymbol{V}_h \, \mathrm{d}x = -\int_\Omega \nabla p_h^i \cdot \boldsymbol{V}_h \, \mathrm{d}x, \quad \boldsymbol{V}_h \in U_{0,h}; \tag{A 2}$$

find $\phi_h^i \in V_{0,h}$ such that

$$\int_\Omega \nabla \phi_h^i \cdot \nabla \phi_n \, \mathrm{d}x = \int_\Omega \operatorname{div} \boldsymbol{u}_h^i \, \phi_h \, \mathrm{d}x, \quad \phi_h \in V_{0,h} \tag{A 3}$$

For all $j \in \Gamma$ the coefficient of the operator is obtained by

$$\mathrm{A}_h(i,j) = \int_\Omega (\nabla \phi_h^i \cdot \nabla q_i - \operatorname{div} \boldsymbol{u}_h^i \, q_i) \, \mathrm{d}x$$

The matrix $(\mathrm{A}_h(i,j))_{i,j}$ is calculated.

A.2. *Construction of the second member*

It is known that

$$B = \int_\Omega (\nabla \phi_{0,h} \nabla q_h - \operatorname{div} \boldsymbol{u}_{0,h} \, q_h) \, \mathrm{d}x.$$

for $i \in \Gamma$, we define the vector of component B_i by

$$B_i = \int_\Omega (\nabla \phi_{0,h} \nabla q_i - \operatorname{div} \boldsymbol{u}_{0,h} \, q_i) \, \mathrm{d}x.$$

The problem (3.14) is equivalent to the following discrete problem. Find $\lambda_i \in R$ such that

$$\sum_{j \in \Gamma} A_h(i,j) \, \lambda_j = B_i \quad \forall i \in \Gamma.$$

REFERENCES

BEAR, J. 1972 *Dynamics of Fluids in Porous Media.* Elsevier.

BEAVERS, G. S. & SPARROW, E. M. 1969 Non Darcy flow through fibrous porous media. *Trans. ASME* E: *J. Appl. Mech.* **36**, 711–714.

BEAVERS, G. S., SPARROW, E. W. & RODENZ, D. E. 1973 Influence of bed size on the flow characteristics and porosity of randomly packed beds of spheres. *Trans. ASME* E: *J. Appl. Mech.* **40**, 655–660.

BECK, J. L. 1972 Convection in a box of porous material saturated with fluid. *Phys. Fluids* **15**, 1377–1383.

BRISTEAU, J., GLOWINSKI, R., MANTEL, B., PERIAUX, J., PERRIER, P. & PIRONNEAU, O. 1979 *A Finite Element Approximation of Navier–Stokes Equations for Incompressible Viscous Fluids.* Rautmann.

CATTON, I. 1984 Natural convection heat transfer in porous media. *NATO Advanced study Institute on Natural Convection: Fundamentals and Application.* Hemisphere.

CHAUVETEAU, G. 1965 Essai sur la loi de darcy et les écoulements laminaires. Thèse, Toulouse.

CONCA, C. & STEER, D. 1983 Résolution des équations bidimensionelles de Navier–Stokes pour un fluide incompressible et visqueux en régime stationnaire, modules N.S.K.I.N.C. et COTABM; *Brochure MODULEF* 107.

COULAUD, O., MOREL, P. & CALTAGIRONE, J. P. 1986 Effets non linéaires dans les écoulements en milieu poreux. *C.R. Acad. Sci. Paris* **302**, 263–266.

DARCY, H. P. G. 1856 *Les Fontaines Publiques de la Ville de Dijon.* Paris: Victor Dalmont.

DE VRIES, J. 1979 Prediction of non-Darcy flow in porous media; *J. Irrigation Drainage Engng.* **105**, 147–162.

DUPUIT, J. 1863 *Etudes Théoriques et Pratiques sur le Mouvement des Eaux.* Paris: Dunod.

FORCHHEIMER, P. 1901 Wasserbegung dusch Baden. *VDIZ.* **45**, 1782–1788.

GLOWINSKI, R. 1984 *Numerical Methods for Nonlinear Variational Problems.* Springer.

GLOWINSKI, R. & PIRONNEAU, O. 1978 Approximation par éléments finis mixtes du problème de Stokes en formulation vitesse-pression. *C.R. Acad. Sci. Paris* **286**, 181–183; 225–228.

GLOWINSKI, R. & PIRONNEAU, O. 1979 On a mixed finite element approximation of the Stokes problem (I): convergence of the approximate solutions. *Numer. Maths* **33**, 397–494.

IRMAY, S. 1958 On the theoretical derivation of Darcy and Forchheimer formulas. *Trans. Am. Geophys. Union* **39**, 702–707.

JOSEPH, D. D., NIELD, D. A. & PAPANICOLAOU, G. 1982 Non linear equation governing flow in a saturated porous medium. *Wat. Resour. Res.* **18**, 1049–1052.

MODULEF 1984 *Un Code Modulaire d'Eléments Finis "Cours et Séminaires". INRIA Rep.*

NIELD, D. A. & JOSEPH, D. D. 1985 Effects of quadratic drag on convection in a saturated porous medium. *Phys. Fluids* **28**, 995–997.

POLAK, E. 1971 *Computational Methods in Optimization.* Academic.

THOMASSET, F. 1980 *Implementation of Finite Element Methods for Navier–Stokes equation.* Springer.

WHITAKER, S. 1969 Advances in the theory of fluid motion in porous media. *Indust. Engng Chem.* **61**, 14–28.